CCFE
CULHAM CENTRE FOR FUSION ENERGY

UK Atomic Energy Authority

UKAEA-CCFE-PR(18)28

M. Fitzgerald, J. Buchanan, S. E. Sharapov, V. G. Kiptily, M. Sertoli, G. Szepesi, J. Boom, R. Akers, D. King and JET contributors

# Full-orbit and drift calculations of fusion product losses due to explosive fishbones on JET

# Full-orbit and drift calculations of fusion product losses due to explosive fishbones on JET

M. Fitzgerald,[1] J. Buchanan,[1] S. E. Sharapov,[1] V. G. Kiptily,[1] M. Sertoli,[1] G. Szepesi,[1] J. Boom,[1] R. Akers,[1] D. King[1] and JET contributors[1]

*[1]EUROfusion Consortium, JET, Culham Science Centre, Abingdon, OX14 3DB, UK*

This is a preprint of a paper submitted for publication in Nuclear Fusion

# Full-orbit and drift calculations of fusion product losses due to explosive fishbones on JET

M. Fitzgerald, J. Buchanan, S. E. Sharapov, V. G. Kiptily, M. Sertoli, G. Szepesi, J. Boom, R. Akers, D. King, and JET contributors
EUROfusion Consortium, JET, Culham Science Centre, Abingdon, OX14 3DB, UK

## Abstract

Fishbones are ubiquitous in high-performance JET plasmas and are typically considered to be unimportant for scenario design. However, during recent high-performance hybrid experiments, sporadic and explosive fishbones have been observed which correlate with a reduction in performance and main chamber hotspots. Clear evidence has been obtained of fusion products being non-resonantly ejected from the plasma by the fishbones. In this work, we present detailed calculations of the motion of fusion products in the presence of fishbones using all available information on the nature of the fishbones observed. Using careful reconstruction of the equilibrium, measurements of the perturbation, and drift and full-orbit calculations, we will show that the fusion product losses can be well modelled by a linear MHD internal kink mode structure. In the drift calculations, the energy content of those losses is insufficient to explain the observed hotspots, however full-orbit calculations show that a combination of magnetic-moment scattering, and wall proximity can produce a significant loss of fusion products at the observed location of the hotspot.

## Introduction

The hybrid scenario on the JET tokamak is being developed to achieve long pulses at high performance in future deuterium-tritium experiments [1]. The scenario is characterised by a safety factor $q$ close to unity at the magnetic axis and low magnetic shear $\frac{r}{q}\frac{dq}{dr}$. The combination of strong thermal pressure and weak magnetic stabilization makes the configuration susceptible to instability, and these instabilities are typically encountered as the limits of a given tokamak's performance are approached. Neoclassical tearing modes (NTMs) are often observed to degrade the fusion yields in JET hybrid scenarios, requiring fine adjustments in scenario design for each attempt at high fusion power to avoid them. Explosive fishbone oscillations are also observed due to the presence of energetic particles from neutral beam and radio frequency heating. The fishbones are clearly responsible for fusion product losses [2][3], but perhaps more concerning is the presence of main chamber hot-spots during some of the recent hybrid experiments; are the observed fusion product losses due to fishbones sufficient to explain the hot-spots?

In scenarios with a safety factor below $q = 1$, the sawtooth instability occurs with an $n = 1$ toroidal and predominantly $m = 1$ poloidal 'kink' spatial periodicity. Maintaining the safety factor at or above unity is effective in preventing the sawtooth instability, and the presence of strongly

anisotropic fast particles contributes a precessional magnetic moment which also tends to stabilize this kink instability[4]. However, the characteristic precessional times of the tens of $keV$ particle orbits become resonant with an oscillatory version of the kink mode, meaning that the very same anisotropic fast particles that stabilize the sawtooth instability can excite a fishbone oscillation [5][6][7].

Although sharing a similar kink spatial profile to the sawtooth and other '1/1 activity', the fishbone oscillation is distinct in that it exhibits a real wave frequency in the plasma frame. This real frequency induces an electric field and alters the wave-particle resonance condition from that for the zero-frequency tearing-modes. For a low-$\beta$ conventional tokamak such as JET, the fishbone has been identified as an "internal kink mode" from the linear MHD theory which requires a $q = 1$ surface to exist [8], however theory also predicts [9] that for sufficiently large $\beta$ and low magnetic shear, pressure may drive an "infernal kink mode". The significance of the infernal solution is that it produces a perturbation that extends beyond the location of the $q = 1$ surface, and the increased influence of higher poloidal harmonics.

## Experimental setup and observations of mode activity

Our work in this paper focuses on detailed analysis of experimental observations published earlier [2]. Here we repeat key observations as an introduction to our analysis.

We consider a recent good case of the hybrid scenario on JET with ITER-like wall, with equilibrium magnetic field and current $B/\ I$ = 2.8 T/ 2.2 MA, and $\beta_N$ ~ 2.6 (discharge #92394). Figure 1 displays the main plasma parameters in this discharge and shows the onset of sporadic large amplitude fishbones.

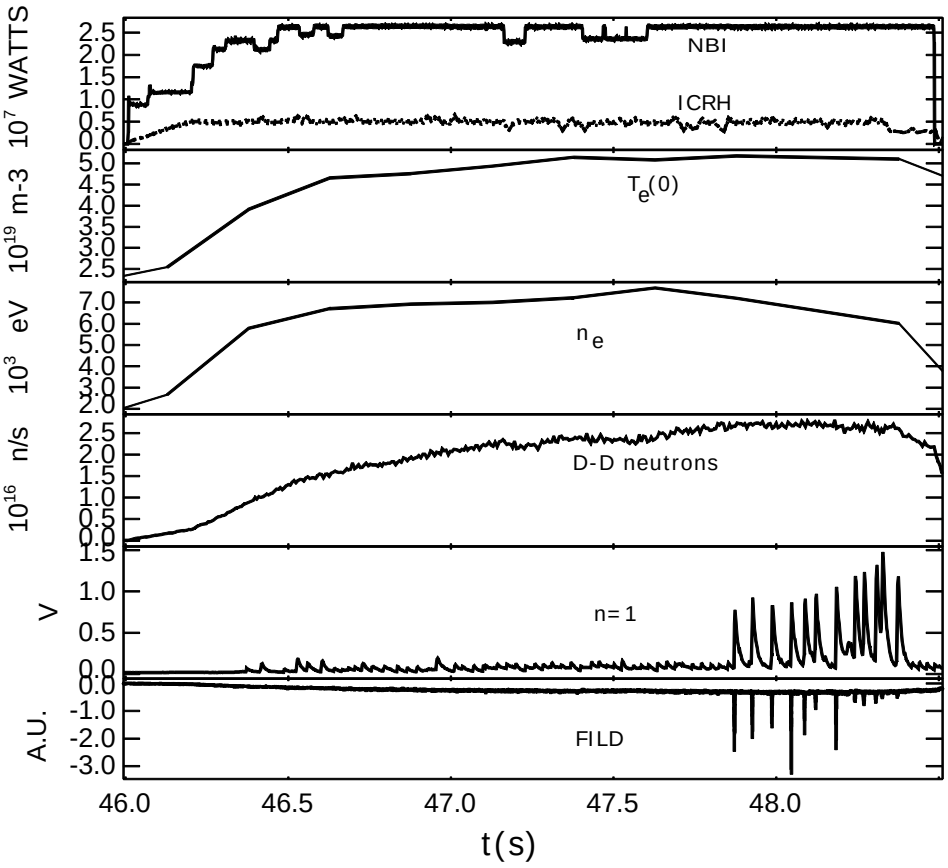


*Figure 1: High performance hybrid scenario #92394. From top to bottom: NBI and ICRH power wave-forms; line-averaged electron density measured with interferometry line-of-sight through the magnetic axis; electron temperature measured with ECE on the magnetic axis; D-D neutron rate from fission chambers; n=1 MHD activity; fast ion loss detector signal.*

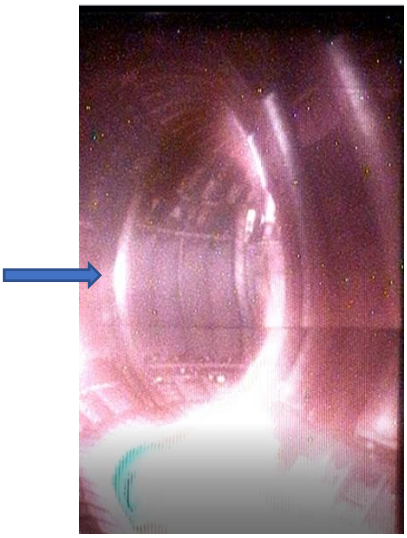

*Figure 2: Visible camera frame taken during fishbone activity for discharge #92394. A hotspot is evident on the outboard poloidal limiter, indicated with the arrow.*

Coherent losses at the fishbone frequency are measured on the fast ion loss detector (FILD)[10]. In addition, main chamber hotspots are evident on the outboard poloidal limiters (Figure 2). The hotspots were sufficiently intense as to trigger machine protection systems and terminate the pulse.

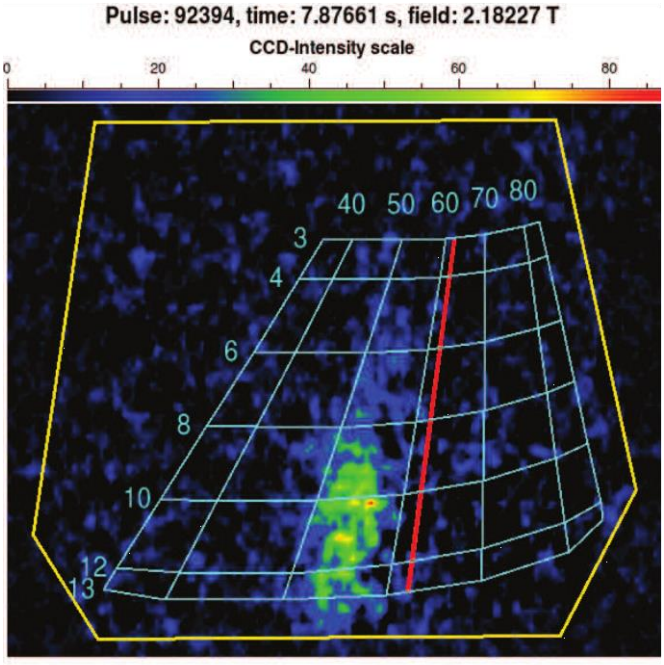


*Figure 3: FILD data from discharge #92394 showing fast ion losses as functions of the pitch-angles in the range* $40° - 80°$ *and Larmor radii 3 cm- 13 cm. Only the difference in signal with and without fishbones is shown. The pitch-angle corresponding to the ICRH H-minority fast ions is shown in solid red. Published in [2].*

The maximum fast ion losses are measured to be associated with the pitch-angle of $55°$ and Larmor radii of 8-13cm (Figure 3). These losses are unlikely to be associated with the ICRH-accelerated hydrogen (H) minority ions, since such ions have pitch-angles near $63°$ (shown with red line) for the on-axis ICRH used in this discharge. Backwards full-orbit modelling (Figure 4) shows that the losses detected are associated with the highly energetic D-D fusion products (3 MeV protons and 1 MeV

tritons), not with H minority ions. The fusion products are lost mostly from the high-field side region of the plasma, close to the trapped-passing boundary.

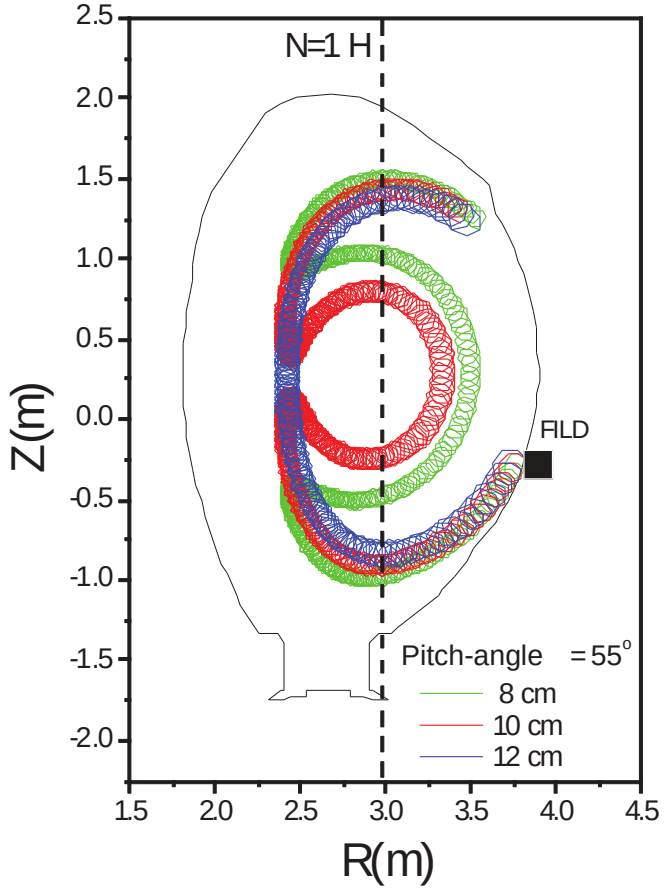


*Figure 4: Full-orbit "backward" modelling for fast ion losses at the position of Fast Ion Lost Detector (FILD). The approximate location of the fundamental H-minority ICRH resonance is shown with the dashed line. Published in [2].*

## Equilibrium reconstruction and predicted mode structure

Equilibrium reconstruction using the EFIT code on JET typically requires the use of internal constraints such as Faraday rotation, motional Stark effect and pressure [11]. In the hybrid scenario, the low shear in the core would imply an unfavourably large uncertainty in the inferred position of the $q = 1$ rational surface for any EFIT reconstruction. The tactic employed in this study was to further constrain the equilibrium using measurements of MHD markers. Figure 5 is a Fourier spectrogram coloured by toroidal mode number. The relevant markers evident in this plot are a $4/3$ NTM at ~45kHz and a 2/1 mode at ~8kHz.

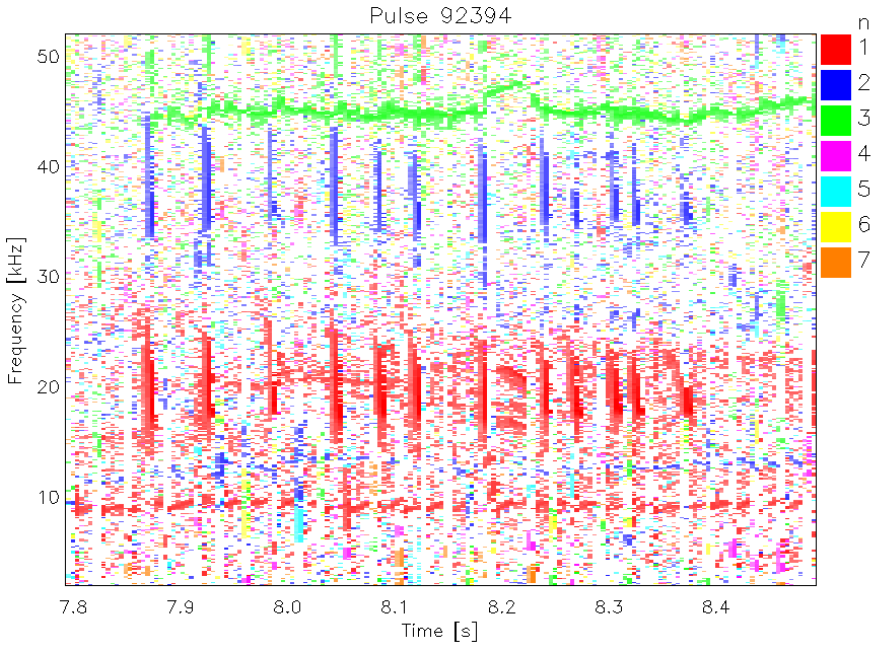


*Figure 5: Fourier spectrogram taken from fast magnetics, with modes coloured by inferred toroidal mode number.*

The most important MHD marker in the case that we present here is the sawtooth inversion radius in electron temperature, as measured through electron cyclotron emission (ECE). Figure 6 contains plots of the time-trace of electron temperature for a set of radial channels. Distinctive sawteeth periodicity and inversion are clearly visible shortly after the time of the first fishbone at 47.8s.

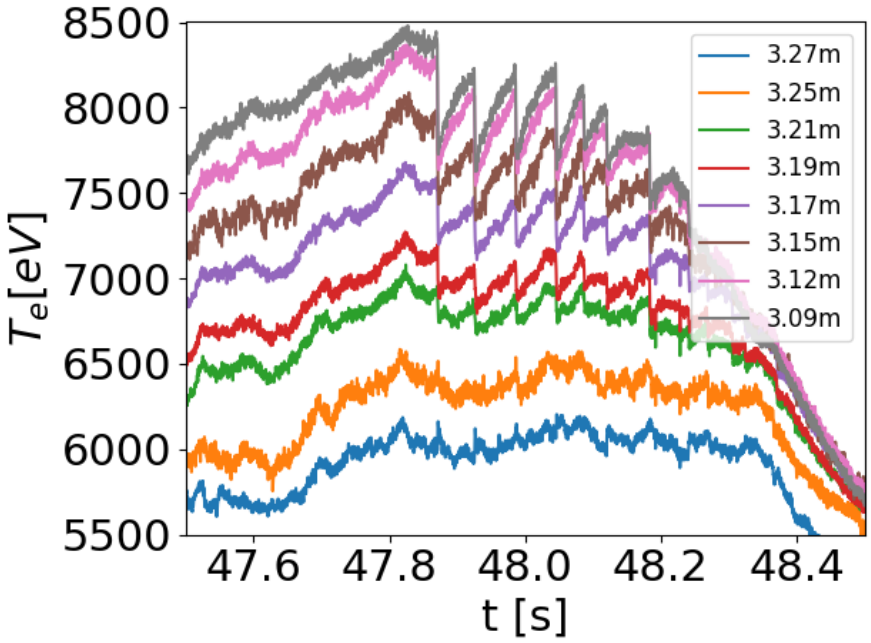


*Figure 6: Electron temperature time-traces measured through electron cyclotron emission at radial locations around the sawtooth inversion radius. Temperature decreases with increasing major radius. Discharge #92394*

The ECE diagnostic on JET requires knowledge of the local magnetic field in order to calibrate the radial position of the channel. This calibration in turn should depend weakly on the equilibrium reconstruction. Convergence in calibrated radial position for this case occurred after a single

reprocessing of this consistency loop. A consistency check between equilibrium and ECE was the requirement that electron temperature be a flux function. Figure 7 is a plot comparing the electron temperature measured on the inboard and outboard midplane as a function of flux-surface label (outboard major radius was chosen to label the poloidal flux surfaces in the plot). The degree of asymmetry present suggests an error in radial position of $\pm 2cm$ reduced from $\pm 5cm$ in a similar plot before reprocessing.
Clearly evident in Figure 7 is the flattening of electron temperature at the location of a $4/3$ NTM. The location of the tearing mode was confirmed using a cross-correlation technique with fast magnetics [12] , detecting a phase shift at the same location, indicative of a magnetic island. The location of the 2/1 mode in Figure 5 was also confirmed using the same technique.

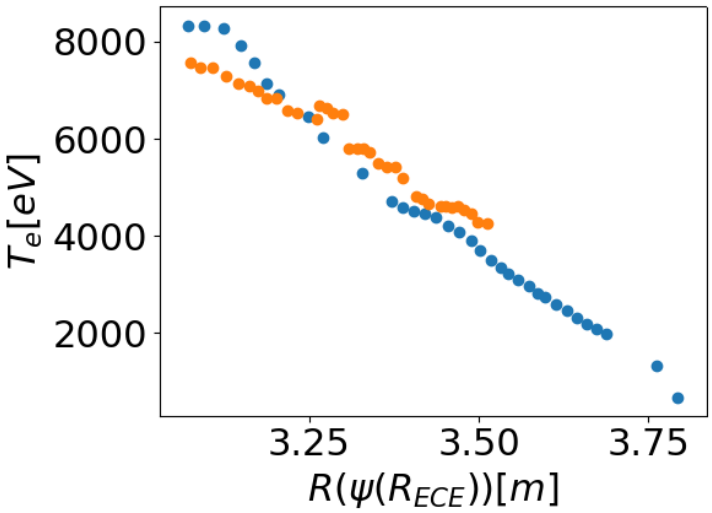


*Figure 7: Calibrated ECE radial profile of electron temperature versus flux label. The flux label is expressed as a radial position on the outboard midplane. Note the plasma boundary is at approximately 3.8m. Orange denotes measurements on the high-field side. Discharge #92394*

The three locations obtained, $3.25 \pm 0.02m$ for sawtooth inversion, $3.42 \pm 0.02$m for the 4/3 and $3.65 \pm 0.05m$ for the 2/1 modes, constrained the value of safety factor to be $q = 1,1.33,2.0$ respectively. EFIT was re-run with the usual internal constraints, but with particular care to satisfy the measured $q$ constraints. Even when using the usual internal constraints, some freedom still remains with EFIT reconstruction in specifying the prior assumptions for allowed forms of the plasma current or for the relative weights of various measurements. To manually obtain a $q$ profile that agrees with the measured values, we exploited this ambiguity by adjusting the relative weighting factor of the imposed internal pressure constraint by $\sim 20\%$ until a satisfactory match with MHD constraints was obtained.

## Assumed form for the fishbone

Using the carefully obtained equilibrium, a stable linear internal kink mode was computed using the ideal MHD MISHKA-1 code [13]. The resulting eigenmode is shown in Figure 8.

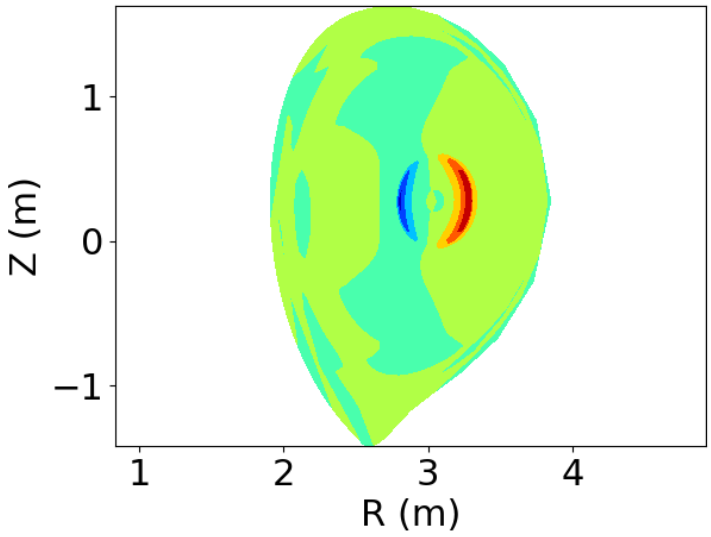


*Figure 8: Electrostatic potential of linear MHD internal kink mode used to model the fishbone*

The solution retains up to 20 poloidal harmonics, but it is obvious from the figure that the eigenmode is dominated by $m = 1$. Although it is predicted that fishbones will nonlinearly evolve in mode structure [14][15], we assume that the nonlinear fishbone mode can be well modelled by the linear MHD mode to the extent required to predict prompt fast ion losses. In the calculations that follow, we will be assuming large amplitudes for the perturbation which will result in stochastic fast ion motion. Under such circumstances, we expect only the radial extent of the mode to alter conclusions made about particle transport, rather than the detailed mode structure.
Soft X-ray (SXR) measurements of perturbed intensity at the instantaneous fishbone frequency provide line-integrated measurements of the fishbone radial extent. The MISHKA mode structure as a function of normalized toroidal flux at $\rho$ is provided in Figure 9 for direct comparison with perturbed intensity in Figure 10. Both the prediction and the measurements show a clear boundary for the perturbation at $\rho = 0.3$ on the outboard midplane. The measured and modelled edge of the fishbone structure are in very good agreement, and the shape is somewhat less acute in the measurements as could be expected from the convolution with line-of-sight and equilibrium density effects, but could also imply a larger value of shear inside $q = 1$ than our computed equilibrium. Nonlinear theory also predicts a smoothing of the linear fishbone profile [16].

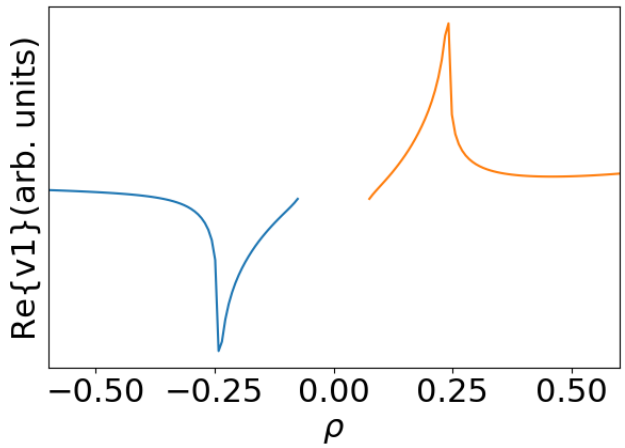


*Figure 9: Perturbed radial fluid velocity as computed by MISHKA, summed over poloidal harmonics and remapped onto normalized root toroidal flux ρ (with negative values denoting high field side).*

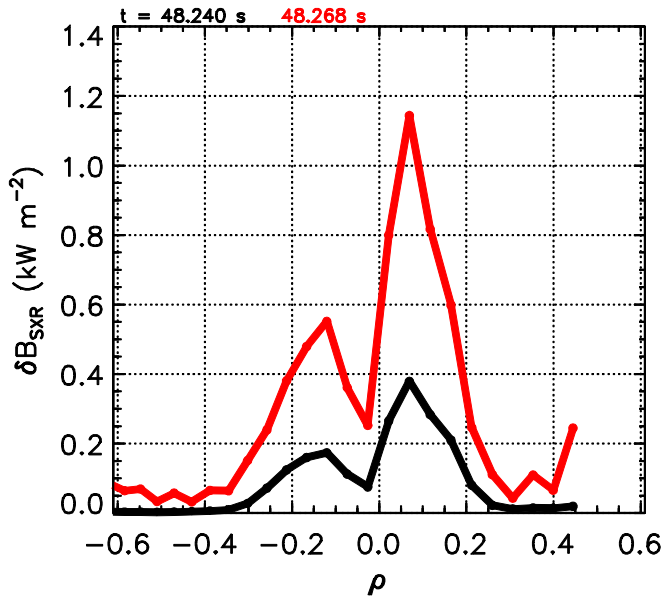


*Figure 10: SXR measurements of perturbed intensity as a function of normalized root toroidal flux, taken at two different times during two different fishbones. Discharge #92394*

The measured perturbation phase given in Figure 11 shows a clear $\pi$ phase change between inboard and outboard sides confirming the predominant $m = 1$ poloidal structure. This supports the assumption that there is dominance of the $m = 1$ component in the nonlinear phase of the fishbone comparable to the linear internal kink mode.

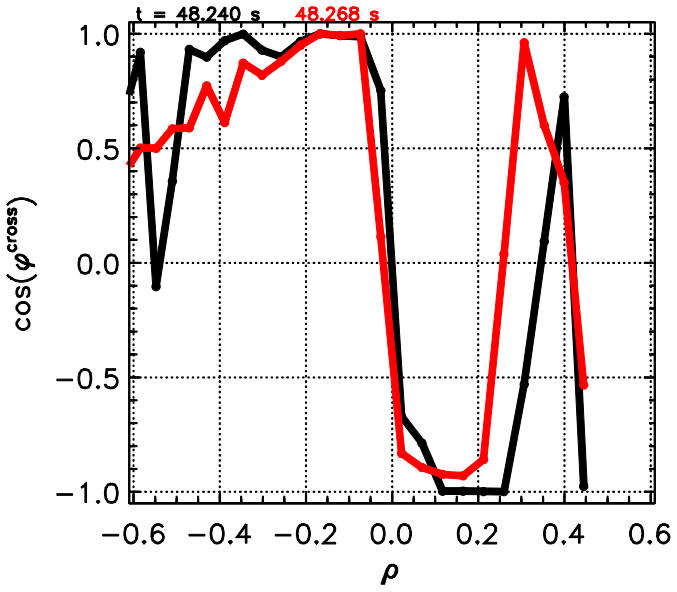


*Figure 11: SXR measurements showing phase change of perturbed intensity as a function of normalized root toroidal flux, taken at the same times as the previous figure. Discharge #92394*

These SXR measurements rule out the more sophisticated “infernal” modes predicted by theory as being a good description of the fishbone in this high-performance hybrid experiment. On the contrary, these fishbones do not require vanishing shear and do not exist where $q > 1$.

In the sections that follow, we will show that the localisation of the mode to the core significantly reduces the types of particle orbits which may be lost as a result of these fishbones, thereby limiting the resulting fast particle losses.

## Calculation of unperturbed orbits

To understand the nature of the observed fusion product losses due to the fishbone, it is necessary to first characterise the confined motion of unperturbed orbits. Confined orbits in the axisymmetric tokamak may be labelled uniquely by invariants of motion: energy $E$, magnetic moment $\mu$, toroidal canonical momentum $P_\phi$, with an additional parameter, $\sigma = sgn(v_\parallel)$, the sign of the particle velocity parallel with the magnetic field. On JET, the toroidal components of the plasma current and magnetic field are in the same direction (clockwise from above). This is also the same direction as the neutral beams and typical ion diamagnetic drift. For all confined equilibrium orbits, $\sigma$ is either also an invariant of the motion or, in the case of trapped particles, a redundant label. For this work, we chose a related set of invariants $(E, \Lambda, +Z_{R=R0})$. The invariant pitch $\Lambda \equiv \frac{\mu B_0}{E}$ is a practical measure of the maximum field encountered by the particle and consequently the minimum value of major radius $R$. The value of the cylindrical coordinate $Z$ taken directly above the magnetic axis $+Z_{R=R0}$ is taken as a more useful choice than $P_\phi$ for this work. In the phase-space plots that follow, we will omit the embellishments in the notation for this invariant and simply write $Z$.

A number of drift calculations using the HAGIS guiding-centre code [17] were carried out, and we have already published some results [2]. We have also recently developed the HALO (HAgis LOCust) code which takes mode structure from MISHKA in the same manner as HAGIS. HALO tracks the particle motion in full-orbit using LOCUST, allowing tracking even beyond the separatrix until reaching the plasma facing components. Detailed benchmarking of the new HALO code against HAGIS has been carried out but those results are a distraction here, and will be detailed in a subsequent publication.

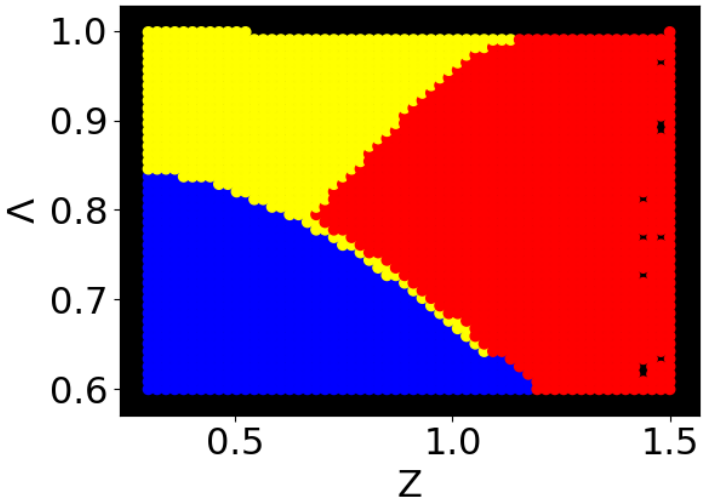


*Figure 12: Orbit classification as a function of orbit invariants for 3MeV protons travelling counter-field as calculated with guiding-centre model HAGIS. Blue denotes passing, yellow trapped and red lost.*

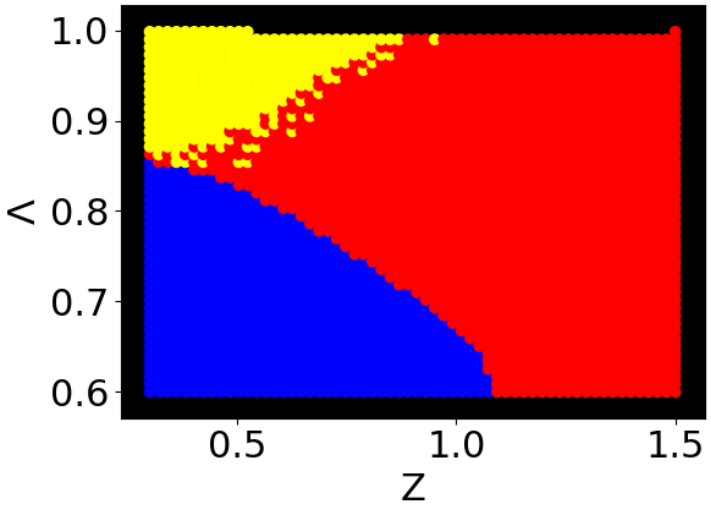


*Figure 13: Full-orbit calculation of unperturbed topologies using LOCUST with a wall model. The proximity of the wall to the separatrix results in losses of fusion products even though the guiding centre motion is still confined*

Figure 12 is a scatter plot in phase space showing the orbit classification for 3MeV protons travelling counter-field, as a function of the orbit invariants $(+Z_{R=R0}, \Lambda)$. The topology boundaries between trapped, passing and lost particles meet at a triple-point and this small region of phase space is chosen for the plot, as this will have significance for our problem. We have also omitted a similar plot for the co-travelling particles. The energy chosen is the birth energy for the fusion products, which in this case corresponds to fast protons in the D-D reaction. Fast triton fusion products at $1MeV$ were also measured [2] but follow the same orbits so we will make no more explicit mention of them.

The HAGIS drift calculation was repeated with the full-orbit LOCUST code using the same guiding-centre locations. The same results for orbit topologies were obtained and are not shown here. However, the additional physics of full-orbits allowed the inclusion of a wall model. Figure 13 including the wall model shows that although barely confined guiding centres remain inside the separatrix in the drift model, the Larmor radius of the fusion products is sufficiently large as to impact the wall on the outboard midplane. The Larmor radius of fusion products encountering the nearby limiter causes a shift in the critical loss triple-point region inwards. We have chosen to load our particles at fixed gyrophase for easier comparison to the drift code HAGIS, so these boundaries between trapped, passing and lost will blur when gyrophase is varied. Although the large fishbone amplitudes assumed in our calculations can create significant deviations in particle orbits, we are seeking to study deviations which ultimately result in a loss, not merely a redistribution. We are only concerned with regions of phase-space that are associated with boundaries between confinement and loss.

If we were to plot the full axis in $\Lambda$ in Figure 12, most of the figure would show confined counter-passing orbits that transition to loss orbits only at large values of $Z$. In a drift picture, the magnetic moment of the particles is invariant, so variations in $\Lambda$ are assumed small. Fusion products are overwhelmingly not produced at regions of high $Z$, and even if they were, the fishbone that we are studying has been demonstrated to exist only at small values of $Z$. The satisfactory confinement of fusion products at low $\Lambda$ is even better for co-passing ions. It is therefore clear that to explain any losses at all in a drift theory, we must study the critical region of phase space around the triple-point

given in Figure 12. That fishbone induced losses should result only from this small region of phase space already suggests that few particles can be lost by this physics mechanism.

A selection of confined drift orbits near the critical triple-point region is shown in Figure 14. Small changes in radius or pitch change the orbit topology from counter-passing to trapped. This radically changes the time-average position of core localised particles due to the large orbit width. At these values of $Z$, the orbits are also barely confined if not lost. It is notable that barely confined fusion products are most likely to be lost along the midplane, with wall impacts occurring further below the midplane for particles deeper in the loss region of phase space. As well as showing the particle orbits, Figure 14 also shows the perturbed electrostatic potential encountered by the critical orbits. The guiding centres of the critical orbits match almost perfectly with the location of the fishbone, indicating that those particles which are the most likely to be lost due to a topology change happen to be precisely the same particles which enter regions with the strongest perturbing fields.

Having established the nature of unperturbed orbits which are the most likely to be lost due to interaction of a fishbone, in the next section we will present the calculations of orbits with the inclusion of the perturbing fields.

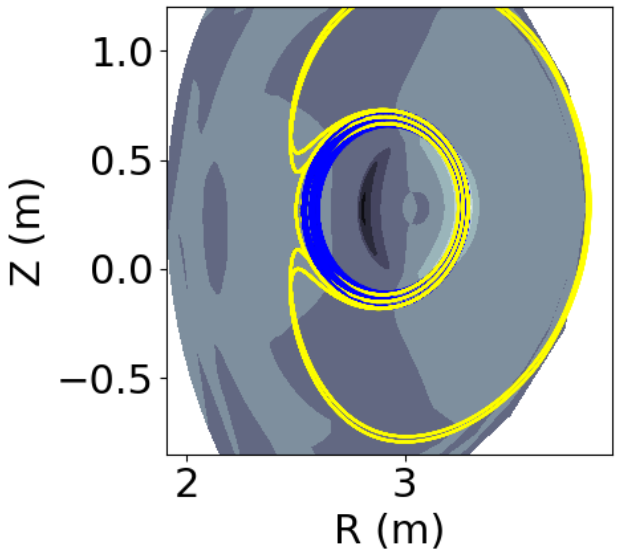


*Figure 14: A selection of 9 confined unperturbed guiding centre orbits from HAGIS chosen near the triple-point. The orbits are overlaid on a plot of the fishbone electrostatic potential. Blue denotes passing and yellow trapped .*

## Calculation of perturbed orbits and physical mechanism behind observed losses

The linear MHD analysis of a well constrained equilibrium, as we have shown from SXR measurements, provides a satisfactory description of the spatial structure of the mode, but does not supply all required information; namely the amplitude of the mode and the mode frequency.
The mode frequency governs the electric field and is responsible for any change in the particle energy, as magnetic perturbations do no work. It is important to note that the orbits of the fusion products have transit and precession frequencies much larger than the frequency of the fishbone. The particles do not resonate with the mode and thus behave as test particles undergoing quasi-linear diffusion rather than convective wave-particle holes and clumps.
The frequency evolution of the fishbones as measured from magnetics is given in Figure 15. The fishbones chirp downward in frequency from $25kHz$ to $16kHz$ in the lab frame. The latter frequency corresponds very well to measurements of the core plasma rotation obtained from charge-exchange spectroscopy, the large rotation owing to the strong beam heating in this high-performance pulse. The rapid frequency chirp to nearly zero frequency in the plasma frame suggests a strongly nonlinear mode with large amplitude. In the absence of more direct measurement of amplitude, we estimated a very large value of $\frac{dB_r}{B_0} = 1\%$. Beyond this value, the fishbone becomes comparable to the equilibrium poloidal field and the plasma is likely to disrupt, so this was the largest order-of-magnitude estimate that we expected to be reasonable. Taking the bottom of the frequency chirp to be the plasma rotation frequency, we inferred the mode frequency in the plasma frame to be $9kHz$. The modes lasted for $3ms$ in total, with a mode envelope which was deemed sufficiently small to justify neglecting its additional contribution to the electric field. The mode was therefore taken as a constant $9kHz$ for a full $3ms$ to give a larger estimate of perturbation to particle orbits.

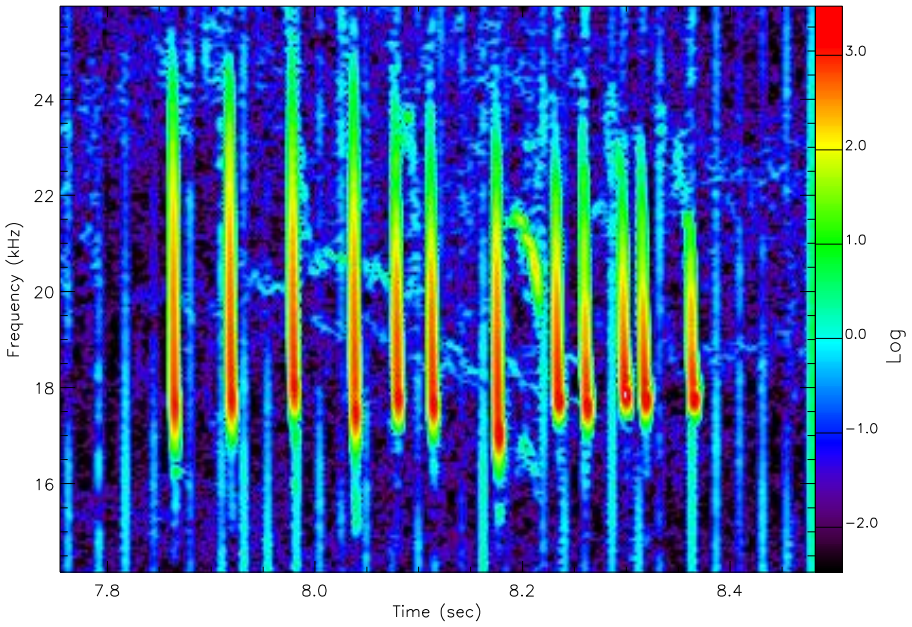


*Figure 15: Fourier spectrum from magnetic pickup coils showing fishbone frequency chirping in discharge #92394*

The presented model for the fishbone was included in both the HAGIS and HALO codes and the orbits reclassified after perturbation. The perturbed orbit topology was obtained by constructing a similar graph to Figure 12, and a plot of where the orbit character changed due to the fishbone is given in Figure 16.

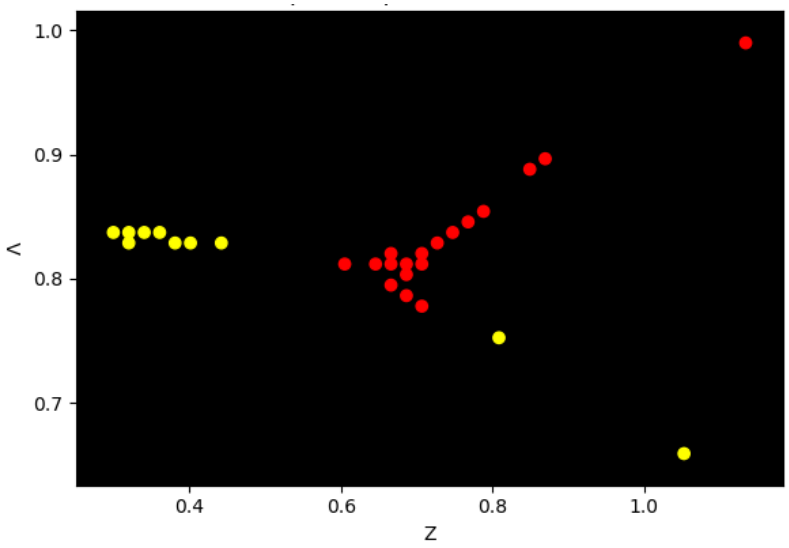


*Figure 16:HAGIS drift calculations showing the difference between two plots of orbit classification of particles, one with and the other without the presence of the fishbone, colouring as before. HAGIS assumes magnetic-moment conservation and ignores FLR effects. From [2]*

The drift calculation shows a very small region in phase space near the topological boundary where the fishbone changes the orbit character to create a loss. At low frequencies ignoring FLR effects, the magnetic moment $\mu$ is expected to be well conserved. The remaining equilibrium invariants in the energy and momentum form a new invariant

$$K \equiv E - \frac{\omega}{n} P_\phi (+Z_{R=R0}).$$

The break in toroidal symmetry is responsible for the change in canonical momentum, and the induced electric field produces a proportional change in the particle energy through the frequency. The change in energy due to the perturbation is a small proportion of the total energy of the particle. Only a small change in canonical momentum (i.e. a small change in $Z$) is required to create a loss, so the change in energy due to the mode is also small. The combination of $\mu$ and $E$ conservation leads to $\Lambda$ being well conserved in the drift calculations. The result is that the difference plot in Figure 16 clearly follows the location of the boundary in Figure 12. The loss mechanism in the drift picture is that trapped, barely confined banana orbits are shifted slightly in radius due to the mode and cross the separatrix resulting in loss.

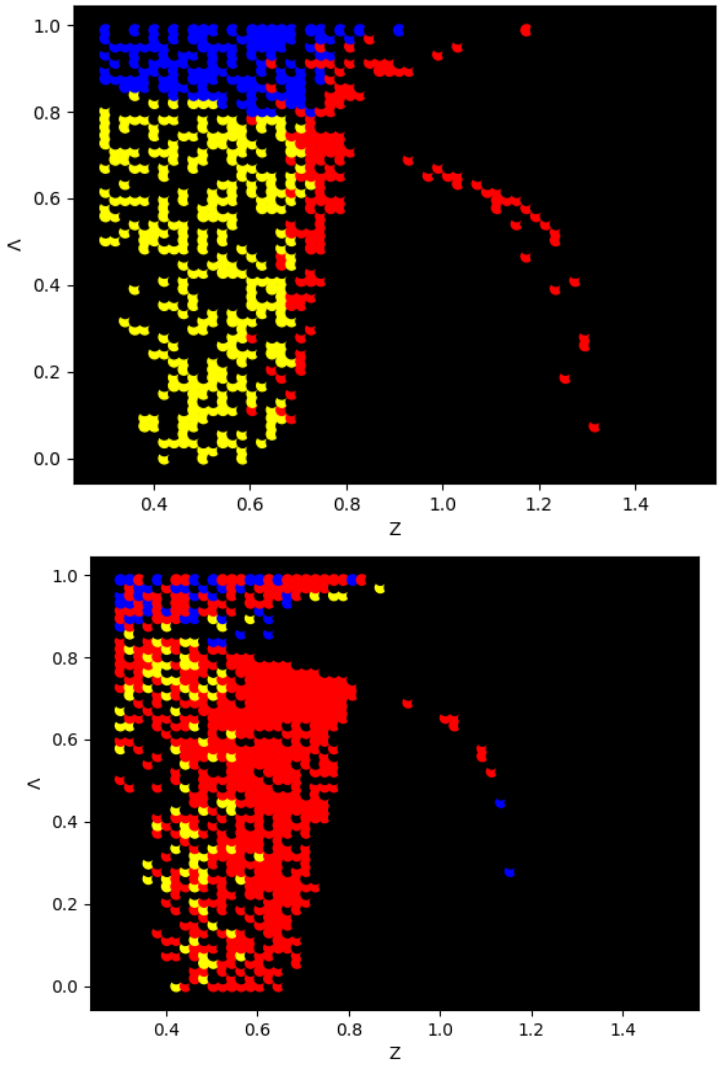


*Figure 17: HALO calculation of orbit change due to the fishbone with (below) and without (above) a wall model, colouring as before. A wider range in invariant pitch is chosen to demonstrate the FLR effect of pitch angle scattering.*

The calculation of fishbone changes to orbit topology was repeated with the HALO code over the full counter travelling pitch domain with and without the wall (Figure 17). Fishbone losses for regions close to the triple-point are still observed but a significant randomization is evident where the perturbation is located. This shows the complete breakdown of $\Lambda$ as an invariant. The likely explanation is that the Larmor radius exceeds some of the length scales for the fishbone resulting in the magnetic moment $\mu$ being no longer conserved. This implies that particles undergo random walks both in radial position and pitch angle.

This is a striking difference between the drift and full orbit theories; particles are diffusing in pitch-angle space and ending up crossing the loss boundary. We expect therefore that full orbit calculations of fishbone loss will far exceed those of drift calculations due to the randomization of pitch. Comparing the difference plots with and without the wall, we can also conclude that pitch-angle diffusion will result in a large proportion of fishbone induced losses occurring due to wall proximity to the plasma. The effect of the wall will be to create a hotspot on the outer midplane where the barely confined guiding centre orbits are not confined in the full-orbit treatment.

To illustrate the typical orbit for fishbone losses, we have run HALO for one of the critical orbits near the triple point in the presence of a perturbation (Figure 18). The wall is plotted in the figure but disabled in the tracking for this plot. The fishbone induced loss orbit clearly corresponds to the barely confined guiding centre orbits shown earlier.

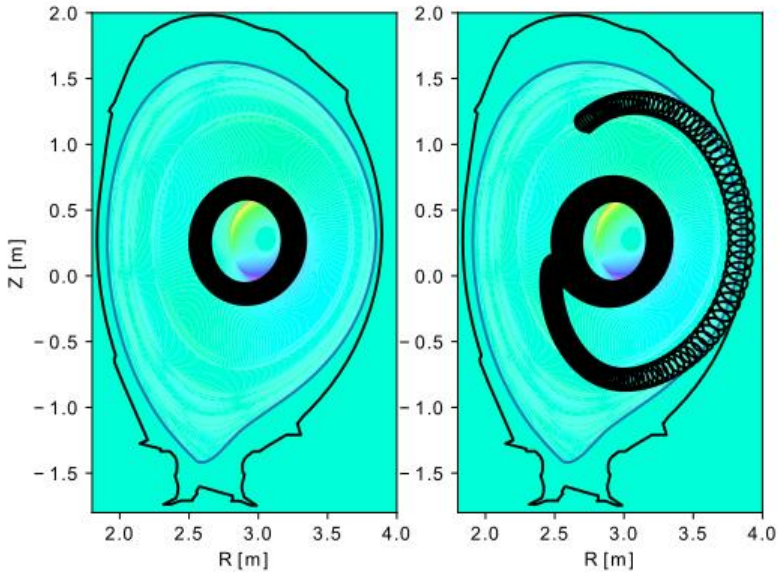


*Figure 18: HALO calculation of a critical orbit undergoing topology change in the presence of a fishbone. Unperturbed (left) and perturbed (right) are shown superimposed on electrostatic potential.*

The barely confined guiding centre orbits are particularly noteworthy for our study here in that our calculations show that they impact the wall where the hotspots are observed in experiment. Both the drift and full-orbit theories predict losses in the same place but disagree radically on how much of phase space is affected.

We have now presented calculations of non-resonant fusion product particle motion in the presence of experimentally constrained fishbones that show that wall and fast ion loss detector impacts are to be expected where they have been observed in experiment. The mechanism is straightforward in that highly energetic counter passing particles near a loss boundary in phase space undergo topology transitions with the associated large deviations in orbit when a fishbone is present. Guiding centre calculations show that perturbation in radius alone is sufficient to produce these topology changes, however full orbit calculations show that magnetic moment perturbations are important due to the narrow magnetic field perturbation near the $q = 1$ rational surface. This results in a rapid velocity space diffusion similar to pitch angle scattering from collisions but on a much more rapid timescale.

Our findings suggest that in a drift model, the volume of phase space sensitive to this effect is small and could not plausibly account for a significant heat loading. On the contrary, full orbit calculations show that pitch-angle scattering and wall proximity combine to transport large numbers of particles in phase space to the wall.

In the next section, we compute heat load estimates based on realistic fusion product source profiles.

## Calculations of heat loads

In this section, we present calculations of the heat losses through the separatrix based on nominal fusion product sources obtained from the TRANSP code. Our purpose is to confirm our reasoning that fishbones do not affect sufficient numbers of particles in the relevant region of phase space to produce losses much beyond those already occurring in stable axisymmetric equilibrium unless full-orbit effects are included. TRANSP is used frequently on JET for scenario development, interpretive modelling and fusion product studies [18], [19] . To approximate a realistic fusion product source distribution function in our calculations, we assumed an isotropic distribution of the form

$$f(\rho, E, \lambda) \approx \frac{1}{2}\delta(E - E_0)\mathrm{PFI}(\rho)$$

where the fusion power density profile 'PFI' was obtained from a JET TRANSP run for similar shot 92395. Calculations of power losses were performed using HAGIS with and without fishbones for both 3 $MeV$ protons and $3.5MeV$ alpha particles.
The alpha particle calculations correspond to slightly different orbit topologies than those presented, but for brevity we omit those test particle orbits here. The slightly higher energy works to increase the number of losses in comparison to the D-D fusion products, due to the larger orbit widths and Larmor radius.

| | **equilibrium** | **with fishbone** | **difference** |
|---|---|---|---|
| **protons** | | | |
| confined | 94.7% | 94.3% | |
| lost | 5.29% | 5.70% | 0.4% |
| **alphas** | | | |
| confined | 93.3% | 92.4% | |
| lost | 6.67% | 7.65% | 1% |

*Table 1: HAGIS calculations of particle losses assuming an initial distribution given by TRANSP*

The results of the HAGIS calculations using the TRANSP radial profile is given in Table 1. The majority confined fraction is to be expected since the profile is used as an energy source in the energy balance calculations in TRANSP; only confined particles contribute significantly to the plasma heating. As expected from test particle orbit calculations presented earlier, the addition of the fishbone makes a tiny contribution to the overall losses in the guiding centre calculation.

| | equilibrium | with fishbone | difference |
|---|---|---|---|
| **protons** | | | |
| confined | 91.7% | 66.2% | |
| lost | 8.26% | 33.8% | 25.5% |

*Table 2: HALO calculations of particle losses. Wall proximity and magnetic-moment scattering result in significant losses during the fishbone.*

The results of full-orbit HALO calculations using the TRANSP radial profile is given in Table 2. The increase in equilibrium losses is attributable to the wall proximity losses. As anticipated, a large proportion, 25%, of the isotropic fusion products are lost via diffusion in magnetic moment over the timescale of the fishbone. Figure 19 shows the final position of particles in the HALO simulation with and without the fishbone.

We stop short of projecting alpha particle losses DT experiments here until we have a more concrete extrapolation of fields and currents, and a more thorough examination of this new pitch-angle scattering effect for different fishbone amplitudes, which is our largest uncertainty. Clearly when megawatts of fusion power are concerned, it pays to be more careful.

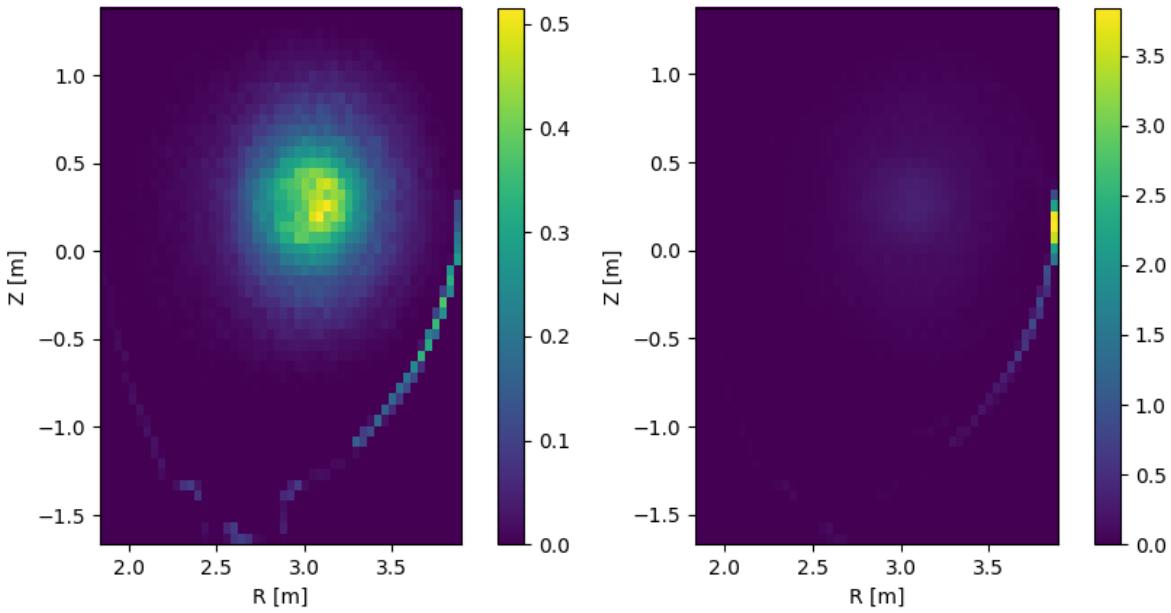


*Figure 19: HALO calculations of TRANSP fusion product numbers in equilibrium (left) and with the mode (right). A combination of magnetic-moment scattering and wall proximity result in a fusion product induced hotspot on the outer midplane during a fishbone. Scale is normalized as a percentage of D-D fusion product power.*

## Conclusions and future work

We have presented detailed calculations of the effect of fishbones on non-resonant fusion product from the D-D reaction in order to explain measured fusion product losses and to assess the likelihood that correlated main chamber hotspots are caused by the same losses. We carefully

determined the radial extent of the fishbone to be localised in the core using inference of $q$ profile and measurements from SXR cameras. The fishbone is measured to resemble the linear MHD internal kink mode structure over the entire nonlinear phase. This fundamental constraint on the localization of the fishbone immediately limits the class of particle orbits which may be ejected from the plasma. The ejection of particles is limited to those whose orbit width plus Larmor radius exceeds the distance from the $q = 1$ rational surface to the separatrix.

This orbit-width is a function of the poloidal Larmor radius and will therefore be a function of the plasma current and device dimension. On JET, non-resonant particles in the $MeV$ range satisfy that criterion but resonant NBI injected particles do not. On ITER, the linear dimensions and current are sufficient to discount any fishbone induced loss of particles, although we do not make any claims about redistribution, which could be significant; large fishbones clearly lead to stochastic diffusion of non-resonant particles.

Our drift calculations show that only a minority of particles near the trapped-passing-lost triple point will undergo sufficient excursion in their equilibrium constants of motion to change their character to loss orbits. In drift calculations which assume exact $\mu$ conservation, a simple translation of a particle in radius due to perturbation from the fishbone is the mechanism for the topology change.

In full-orbit calculations, the fishbone is sufficiently narrow as to vary significantly over a Larmor radius, leading to randomization of equilibrium invariant $\Lambda$ . The resulting pitch-angle scattering is sufficient over the timescale of a single fishbone, to produce orbit topology changes over the entire pitch angle space. This diffusion in pitch-angle occurs until a particle enters a critical orbit. The critical orbit particles from near the triple-point predicted to be ejected by the fishbone are precisely the same orbits observed on FILD measurements.

Having understood the mechanism and class of particles ejected according to drift and full-orbit calculations, we loaded a realistic particle distribution of fusion products over the full phase space to give quantitative estimates for heat loads. Our conclusion using the drift model was that the large fishbones observed account for a mere $\sim 1\%$ power loss even when considering the alpha particles in the same conditions. In contrast, the full orbit calculations including a wall show a 25% fusion product loss will occur, with a majority on the outboard midplane where the wall is within reach of an ion Larmor radius for a barely trapped particle.

We have thus shown that the drift theory is insufficient to account for observed hotspots due to fusion products, and that a full-orbit theory provides a satisfactory explanation. We expect the losses to be worse for alpha particles, so fishbones clearly need to be taken into consideration in preparation for JET D-T experiments.

The loss of adiabaticity due to singular currents and the associated diffusion in velocity space is, to our knowledge, an important neglected mechanism for fast particle redistribution and loss. Velocity space diffusion due to loss of adiabaticity has been described previously for equilibrium magnetic field minima [20]. On the other hand, that the magnetic moment is not invariant in the presence of short wavelength electrostatic turbulence is somewhat foundational for redefining the invariant in gyrokinetic theory [21]. This effect in the presence of other singular currents, such as those found near tearing modes, warrants further study.

# Acknowledgments

This work has been carried out within the framework of the EUROfusion Consortium and has received funding from the Euratom research and training programme 2014-2018 under grant agreement No 633053 and from the RCUK Energy Programme [grant number EP/P012450/1]. To obtain further information on the data and models underlying this paper please contact PublicationsManager@ccfe.ac.uk*. The views and opinions expressed herein do not necessarily reflect those of the European Commission.

## Bibliography

[1] C. Gormezano, C. D. Challis, E. Joffrin, X. Litaudon, and a. C. C. Sips, "Advanced tokamak scenario development at JET," *Fusion Sci. Technol.*, vol. 53, no. May, pp. 958–988, 2008.

[2] V. G. Kiptily *et al.*, "Fusion product losses due to fishbone instabilities in deuterium JET plasmas," *Nucl. Fusion*, vol. 58, no. 1, p. 14003, Jan. 2018.

[3] C. P. von Thun *et al.*, "MeV-range fast ion losses induced by fishbones on JET," *Nucl. Fusion*, vol. 50, no. 8, p. 84009, Aug. 2010.

[4] F. Porcelli, "Fast particle stabilisation," *Plasma Phys. Control. Fusion*, vol. 33, no. 13, pp. 1601–1620, Nov. 1991.

[5] L. Chen, R. White, and M. N. Rosenbluth, "Excitation of Internal Kink Modes by Trapped Energetic Beam Ions," *Phys. Rev. Lett.*, vol. 52, no. 13, pp. 1122–1125, 1984.

[6] B. Coppi and F. Porcelli, "Theoretical model of fishbone oscillations in magnetically confined plasmas," *Phys. Rev. Lett.*, vol. 57, no. 18, pp. 4–7, 1986.

[7] K. McGuire *et al.*, "Study of high-beta magnetohydrodynamic modes and fast-ion losses in PDX," *Phys. Rev. Lett.*, vol. 50, no. 12, pp. 891–895, 1983.

[8] H. J. de Blank, "Theory of the m= 1 kink mode in toroidal plasmas," Rijksuniversiteit Utrecht, 1990.

[9] J. Manickam, N. Pomphrey, and A. M. M. Todd, "Ideal MHD stability properties of pressure driven modes in low shear tokamaks," *Nucl. Fusion*, vol. 27, no. 9, pp. 1461–1472, Sep. 1987.

[10] S. Baeumel *et al.*, "Scintillator probe for lost alpha measurements in JET," *Rev. Sci. Instrum.*, vol. 75, no. 10 II, pp. 3563–3565, 2004.

[11] M. Brix, N. C. Hawkes, A. Boboc, V. Drozdov, and S. E. Sharapov, "Accuracy of EFIT equilibrium reconstruction with internal diagnostic information at JET," *Rev. Sci. Instrum.*, vol. 79, no. 10, p. 10F325, Oct. 2008.

[12] M. Baruzzo *et al.*, "Neoclassical tearing mode (NTM) magnetic spectrum and magnetic coupling in JET tokamak," *Plasma Phys. Control. Fusion*, vol. 52, no. 7, p. 75001, 2010.

[13] A. Mikhailovskii, G. Huysmans, W. O. K. Kerner, and S. E. Sharapov, "Optimization of Computational MHD Normal-Mode Analysis for Tokamaks," *Plasma Phys.*, 1997.

[14] F. Wang, G. Y. Fu, J. A. Breslau, and J. Y. Liu, "Linear stability and nonlinear dynamics of the fishbone mode in spherical tokamaks," *Phys. Plasmas*, vol. 20, no. 10, p. 102506, Oct. 2013.

[15] A. Ödblom, B. N. Breizman, S. E. Sharapov, T. C. Hender, and V. P. Pastukhov, "Nonlinear magnetohydrodynamical effects in precessional fishbone oscillations," *Phys. Plasmas*, vol. 9, no. 1, p. 155, 2002.

[16] B. N. Breizman and S. E. Sharapov, “Major minority: energetic particles in fusion plasmas,” *Plasma Phys. Control. Fusion*, vol. 53, no. 5, p. 54001, May 2011.

[17] S. D. Pinches *et al.*, “The HAGIS self-consistent nonlinear wave-particle interaction model,” *Comput. Phys. Commun.*, vol. 111, no. 1–3, pp. 133–149, Jun. 1998.

[18] R. V. Budny *et al.*, “Local transport in Joint European Tokamak edge-localized, high-confinement mode plasmas with H, D, DT, and T isotopes,” *Phys. Plasmas*, vol. 7, no. 12, pp. 5038–5050, Dec. 2000.

[19] H. Weisen *et al.*, “The ‘neutron deficit’ in the JET tokamak,” *Nucl. Fusion*, vol. 57, no. 7, p. 76029, Jul. 2017.

[20] I. B. Bernstein and G. Rowlands, “Diffusion in velocity space associated with nonadiabatic changes in the magnetic moment of a charged particle,” vol. 1546, no. 1976, 1981.

[21] J. B. Taylor, “Magnetic Moment Under Short-Wave Electrostatic Perturbations,” *Phys. Fluids*, vol. 10, no. May 2015, p. 1357, 1967.